Thermal effects of the substrate on water droplet evaporation

B. Sobac* and D. Brutin
Laboratoire IUSTI, UMR 7343 CNRS, Aix-Marseille Université, 5 rue Enrico Fermi, 13453 Marseille cedex 13, France
(Received 19 April 2012; published 20 August 2012)

We experimentally investigate the behavior of a pinned water droplet evaporating into air. The influence of the substrate temperature and substrate thermal properties on the evaporation process are studied in both hydrophilic and hydrophobic conditions. Our objective is to understand the effect of thermal mechanisms on the droplet evaporation process. The experimental results are compared with the quasisteady, diffusion-driven evaporation model, which is implemented under the influence of the temperature; the model assumes the isothermia of the droplet at the substrate temperature. The results highlight a favorable correlation between the model and the experimental data at ambient temperatures for most situations considered here. The model works to qualitatively describe the influence of the substrate temperature on the evaporation process. However, with an increase in the substrate temperature, the role of the thermal-linked mechanisms becomes increasingly important; this experiment highlights the need for more accurate models to account for the buoyant convection in vapor transport and the evaporative cooling and heat conduction between the droplet and the substrate. Finally, the experimental data reveal the modification of contact angle evolution as the temperature increases and the crucial role played by the nature of the substrate in the evaporation of a sessile droplet. The influence of the substrate thermal properties on the global evaporation rate is explained by the parallel thermal effusivity of the liquid and solid phases.

DOI: 10.1103/PhysRevE.86.021602 PACS number(s): 68.03.Fg, 68.60.Dv, 68.08.Bc

I. INTRODUCTION

The study of sessile droplet evaporation has been a subject of increasing interest in recent years due to the important role of this process in many new applications. For instance, one can cite DNA mapping [1], ultraclean surfaces [2], self-assembly technologies [3,4], printing and coating technologies [5,6], surface patterning [7], manufacture of new electronic and optical devices [8–10], or medical tests [11–13]. The extensive investigations lead to vital improvements in the understanding and description of the phenomenon [14–17]. Particular emphasis was placed on the problems of wettability during evaporation and the interaction between the two phenomena. However, sessile droplet evaporation is currently a challenging problem of soft matter physics because of the complexity of the associated fluid dynamics, the physical chemistry of the substrate, and the heat and mass transfer.

Numerous studies have been undertaken to understand the influence of substrate surface properties on the wettability of a sessile droplet [18,19]. The surface-free energy and surface roughness are known to be the two key parameters governing the contact angle of the droplet. The awareness of the complementary roles of these two surface parameters has led to the development of textured surfaces in order to produce superhydrophilic [20], superhydrophobic [21–23], or superoleophobic surfaces [24–26].

Related to these surface properties, several evaporation modes have been explored: the constant-angle mode [14,27], in which the contact area of the droplet on the surface vanishes; the constant contact-area mode [14–16,28,29], in which the contact angle vanishes; and the combination of both modes [14,30,31]. A wide range of wettability has also been investigated, from hydrophilic situations [14–16,27,30,32] to hydrophobic and, more recently, superhydrophobic situations [17,32–34]. According to the surface properties, the dynamics and kinetics of evaporation are totally different [32,35,36] because the overall evaporation rate is directly related to the contact angle and the triple-line behavior (see the next section about theory and model). The separated and coupled roles of the triple line and the wettability on the sessile droplet evaporation process have been investigated [32]. All of these investigations considered the spontaneous natural evaporation of a droplet and demonstrated good agreement with quasistatic, diffusion-driven evaporation models, suggesting that thermal effects are negligible. Recently, universal relations for the time evolution of the droplet mass and the time evolution of the contact angle, independent of the droplet size and initial contact angle in the situation of pinned droplet evaporation, have been deduced from the Popov model [17] and correlate well with experimental data [32,33].

Paradoxically, only a few investigations were concerned with the thermal effects of the substrate on the droplet evaporation process. Some authors studied the influence of the thermal conductivity of the substrate on natural droplet evaporation. Ristenpart *et al*. [37] showed that the thermal conductivity is an important parameter that needs to be considered because the ratio of the liquid and solid conductivities can modify the internal flow direction. David *et al*. [38] experimentally observed that an increase in the conductivity of the substrate causes an increase in the overall evaporation rate. This result contradicts the conclusion that thermal effects do not play a role during natural evaporation. Thus, new mathematical and numerical models to generalize the theoretical model of quasisteady, diffusion-limited evaporation were developed by taking into account the thermal effects associated with evaporative cooling [39] and related to the thermal resistance of the substrate [40]. These improvements are notably due to the attention to the variation of the saturation concentration with temperature, hence coupling the problems for the vapor

*benjamin.sobac@polytech.univ-mrs.fr

concentration in the atmosphere and the temperature of the liquid and substrate. Under some conditions, the heat diffusion in the substrate can become the limiting parameter of the evaporation rate [41].

Other studies address the effect of the surface temperature on the droplet evaporation process. Experimentally, Crafton *et al*. [42] and Grandas *et al*. [35] highlighted that the overall evaporation rate still evolves linearly with the wetting radius. Numerically, these studies focused on the evaporation of pinned water droplets in a wetting situation. Girard *et al*. [43] investigated the influence of the heating temperature and the relative humidity on the evaporation process and proposed an empirical law for droplet evaporation time as a function of these parameters assuming a perfectly conductive substrate. Saada *et al*. [44] developed a convection-diffusion model to analyze the effect of buoyant convection in the surrounding air on the heat and mass transfer phenomena during evaporation. These authors observed that the diffusion model always underpredicts the overall evaporation rate and that the deviation increases with the temperature of the substrate. Whereas the previous studies considered a droplet evaporating into air with an imposed temperature at the substrate surface as boundary condition, Sodtke *et al*. [45], for their part, were interested in the situation of a thin drop evaporating into pure vapor on a surface with an imposed heat flux density. A theoretical model of evaporation taking account of the heat conduction in the liquid and solid phases were developed by the authors and reveals a good agreement with their experimental data.

The literature reveals that the previously developed theory, including the thermal effects, is almost exclusively based on the experimental results of David *et al*. [38] which is limited to experiment at ambient temperature. In this paper, we propose to revisit the configuration of David *et al*. [38] and extend the study to the situation of a heated substrate for a wide range of substrate temperatures. The originality of this experiment is to decouple the effects of wetting properties and thermal properties of the substrate. Thus, whereas previously we investigated the role of wetting properties on evaporation by changing the surface energy and the roughness while maintaining the thermal properties constant thanks to nanoscale coatings on the substrate surface [32], here we investigate the influence of the thermal properties of the substrate while keeping the wetting properties the same by using the coating technic. The bulk of the studies presented in the review of literature are limited to contact angles below 90 °C, thus we carry out experiments on a large range of contact angles allowing us to investigate hydrophilic and hydrophobic situations. Experimental data are compared to the quasisteady diffusion-driven evaporation model assuming the isothermia of the drop at the substrate temperature. This comparison permits us to highlights several thermal mechanisms linked to evaporation and their respective contributions in regard of pure mass diffusion mechanism. The range of validity of the classical evaporation model is also discussed. These results are important for a complete modeling of the phenomena.

After a brief overview of the theoretical macroscopic models developed for sessile droplet evaporation in Sec. II and a presentation of the experimental setup and protocol in Sec. III, the results are presented and discussed in Sec. IV. The influence of substrate temperature on geometrical evolution, evaporation rate, and time of evaporation are investigated and compared with theoretical models and numerical simulations in the case of a hydrophilic situation (Sec. IV A1) as well as in the case of a hydrophobic situation (Sec. IV A2). The influence of temperature on the contact angle evolution is discussed in Sec. IV A3. Finally, the last section concerns the influence of the thermal properties of the substrate in the situation of forced evaporation (Sec. IV B).

II. THEORY: MODELS OF DROP EVAPORATION

For a small drop with a contact radius less than the capillary length, the fluid adopts a spherical cap shape because gravitational forces are negligible. Hence, the droplet volume V can be expressed as a function of the wetting radius R and the contact angle θ as follows:

$$V(R,\theta) = \frac{\pi R^3}{3}\frac{(1-\cos\theta)^2(2+\cos\theta)}{\sin^3\theta}. \tag{1}$$

The natural evaporation of a droplet is generally assumed to be controlled by the diffusion of vapor molecules in the gas phase. The evaporative flux from a droplet surface of an evaporating droplet is modeled based on the diffusion of molecules from the liquid-gas interface of the droplet to the surrounding gas phase. Vapor transport by free convection, induced by the density difference between dry and humid air, is assumed to be negligible compared to diffusive transport [46]. The influence of evaporative cooling of the droplet on the evaporative rate is also neglected [39]. Hence, vapor transport occurs mainly by diffusion of water vapor and is characterized by a diffusion time $t_D = R^2/D$, with D as the diffusion coefficient. The diffusion time for water vapor in air is on the order of 10^{-2} s. Evaporation occurs in quasisteady fashion because the diffusion time is smaller than the evaporation time $t_D/t_F \approx 10^{-5}$, which means that the vapor concentration adjusts rapidly compared with the time required for evaporation. The quasisteady, diffusion-limited evaporation is then governed by the steady Laplace equation. The concentration field around the droplet is given by

$$\nabla^2 c = 0. \tag{2}$$

At the interface between the liquid and the vapor, the vapor concentration c is assumed equal to the saturation value c_V. Far above the droplet, the vapor concentration approaches an ambient value of $c_\infty = Hc_V$ where H is the relative humidity of the ambient air. The difference in vapor concentration $\Delta c = c_v(1-H)$ drives the evaporation into the air. The diffusive flux is given by Fick's law: $\boldsymbol{J} = -D\boldsymbol{\nabla} c$. This problem has been solved in the limit of small contact angle ($\theta < 90^\circ$) by Deegan [15] and Hu and Larson [16]. An analytical solution for droplets of arbitrary contact angles has been obtained by Popov [17] using the analytical solution to the equivalent problem of finding the electric potential around a charged lens-shaped conductor [47]. The rate of mass loss from a droplet of arbitrary contact angle is given by

$$-\frac{dm}{dt} = \int_0^R J(r)\sqrt{1+(\partial_r h)^2}2\pi r dr = \pi R D(c_s - c_\infty) f(\theta), \tag{3}$$

where m is the droplet mass, J is the diffusive outflux from the droplet surface, $h(r,t)$ is the droplet height, t is the time, r is the radial coordinate, and

$$f(\theta) = \frac{\sin\theta}{1+\cos\theta} + 4\int_0^\infty \frac{1+\cosh 2\theta\tau}{\sinh 2\pi\tau}\tanh[(\pi-\theta)\tau]d\tau. \tag{4}$$

For a pinned droplet, the volume is a function of θ by the geometric relation presented in Eq. (1). The contact angle evolution can be determined from an ordinary differential equation obtained from Eqs. (1) and (3):

$$\frac{d\theta}{dt} = -\frac{D(c_s - c_\infty)}{\rho R^2}(1+\cos\theta)^2 f(\theta). \tag{5}$$

Once the evolution of θ is obtained by numerical integration, $V(\theta)$ and dm/dt can be derived. Recently, Gelderblom *et al.* [33], introducing the nondimensional mass $\widehat{m} = \frac{m}{\rho R^3}$ and time $\widehat{t} = \frac{c_s - c_\infty}{\rho}\frac{t}{R^2/D}$, showed that mass and contact angle evolutions can be described by the respective universal law for all droplet sizes [33] and initial contact angles [32].

In the situation of forced evaporation, the complete analytical resolution of the equations governing a heated droplet has remained, until now, an open problem. However, the previous model can be extended to include the substrate temperature T_s. A full analytic solution was obtained for a droplet evaporating in the specific case of an isothermal problem. Using previously developed similar assumptions, it is possible to show that the vapor concentration around the droplet is still governed by the Laplace equation. Indeed, at a temperature of 75 °C, the ratio of diffusion time to evaporation time is on the order of 10^{-4}. Assuming the interface is isothermal at the substrate temperature T_s, as the literature has revealed the largest temperature gradients in such systems are smaller than a few degrees [48], the evaporation rate is driven by the difference of vapor concentration $\Delta c = c_v(T_s) - Hc_v(T_a)$ where T_a is the ambient temperature far above the droplet. Hence, Eqs. (3) and (5) are generalized by [43]

$$-\frac{dm}{dt} = \pi DR[c(T_s) - Hc(T_a)]f(\theta), \tag{6}$$

$$\frac{d\theta}{dt} = -\frac{D[c(T_s) - Hc(T_a)]}{\rho R^2}(1+\cos\theta)^2 f(\theta). \tag{7}$$

In the case of a pinned droplet, the evaporation time is expressed by

$$t_F = \frac{\rho R^2}{D\Delta c}\int_0^{\theta_0}\frac{d\theta}{(1+\cos\theta)^2 f(\theta)}, \tag{8}$$

where θ_0 is the initial contact angle.

For small contact angle $\theta \ll 1$ rad, we can show that the contact angle and the volume decrease linearly with time [17],

$$\theta = \theta_0\left(1 - \frac{t}{t_F}\right), \tag{9}$$

$$V = \frac{\pi R^3\theta_0}{4}\left(1 - \frac{t}{t_F}\right), \tag{10}$$

with the evaporation time defined by

$$t_F = \frac{\pi\rho R^2\theta_0}{16D\Delta c}. \tag{11}$$

However, as soon as the initial contact angle is above 40° [16,32], the evaporation rate decreases nonlinearly over time due to the evolution of the function of the contact angle $f(\theta)$. Then, the global evaporation rate $\frac{dm}{dt}|_g$, which is equivalent to the medium evaporation rate during evaporation, is defined by

$$\left.\frac{dm}{dt}\right|_g = \frac{1}{t_F}\int_0^{t_F}\frac{dm}{dt}dt = -\frac{m_0}{t_F}. \tag{12}$$

III. MATERIALS AND METHODS

The experiment essentially involves the evaporation of a water droplet onto a substrate. The droplet is created using a micropipette to control the volume of the droplet, which is gently laid down on the substrate. The droplet evaporates into air inside an experimental cell in PMMA (65 × 135 × 40 mm^3) to avoid any perturbations from potential external flow. The surrounding air temperature T_a, pressure P_a, and humidity H are measured using a weather station (Lufft opus). A schematic diagram illustrating the experimental setup is provided in Fig. 1.

The substrate is an aluminum cylinder (diameter = 10 mm, height = 10 mm) at the top of which is applied a coating of nanoscale thickness by plasma-enhanced chemical vapor

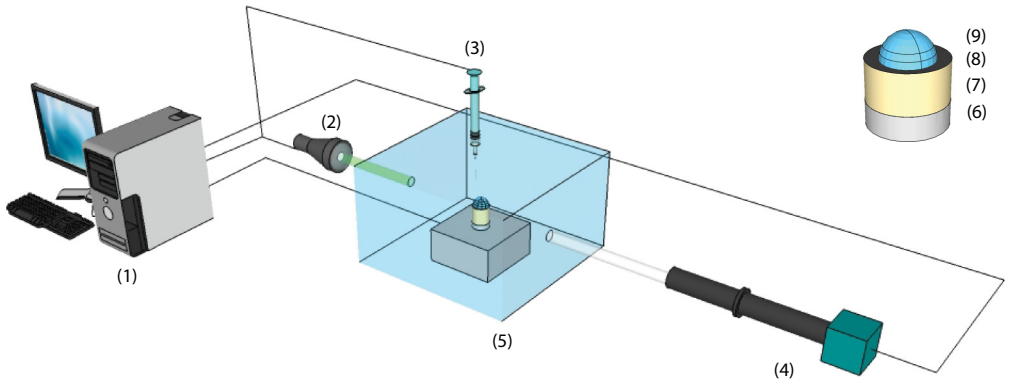

FIG. 1. (Color online) Schematic diagram illustrating the experimental setup, including a computer with drop shape analysis (DSA) software (1), a cold light source (2), a computer controlled syringe (3), a charge-coupled device (CCD) camera fitted with a macrolens (4), and an experimental cell (5). As observed in the inset, the experimental cell includes a heated aluminum block regulated in temperature (6), the substrate (7), coated with a nanoscale layer (8), and the water droplet (9).

TABLE I. Summary of nanocoating processes used in this study.

Material	Notation	Thickness[a]	Roughness[b]	Contact angle
Low-carbon PDMS	SiO_x	4 nm	1.75 μm	$67 \pm 5^\circ$
Perfluorocarbon	PFC	14 nm	1.75 μm	$133 \pm 2^\circ$

[a]Thickness obtained using profilometry.
[b]Root mean square roughness obtained using atomic force microscopy.

deposition (PECVD). The two coatings used in this study are PFC and SiO_x. The PECVD technique, the preparation, and the chemical composition of these coatings were previously presented by Phan *et al.* [49]. These two surfaces were characterized with respect to morphology using an atomic force microscope (Veeco Explorer) and with respect to wettability using a contact angle measurement system (Kruss DSA30). All data are summarized in Tables I and II. These nanocoatings allow for changes in the surface energy of the substrate while maintaining the surface roughness and the thermal properties of the substrate [32]. Estimates of thermal resistances reveal a negligible influence of these coatings on the thermal properties of the substrate. All evaporation on these surfaces was performed with the pinning of the triple line throughout almost the entire duration of the evaporation process due to the relative importance of the surface roughness. The SiO_x coating allows for the study of evaporation in a hydrophilic situation with an initial contact angle $\theta_0 = 67 \pm 5^\circ$ whereas the PFC allows for the study of evaporation in a hydrophobic situation $\theta_0 = 133 \pm 2^\circ$ (see Fig. 2).

To investigate the influence of the substrate temperature T_s, the substrate can be heated from the base with a heated aluminum block ($40 \times 40 \times 20$ mm^3) equipped with two heating cartridges and a platinum probe (Pt 100) on the surface. This latter is fitted with a PID temperature regulator (Omron E5GN) to impose a controlled temperature. The contact is performed via a fine layer of thermal grease (compound silicone Jelt Cm). A range of temperatures from the ambient temperature to 75 °C were investigated.

To investigate the influence of thermal properties of the substrate, the cylinder can be exchanged for cylinders made of other materials including copper, brass, bronze, and polyoxymethylene (POM). All these materials were chosen for their widely different thermal conductivities from insulating (POM) to highly conductive substrates (copper). The relevant physical properties of the substrates used are listed in Table II.

The experimental cell was inserted into the center of a Kruss DSA30 drop shape analyzer. This measurement system allows one to optically obtain the evolution of the droplet base radius R, the contact angle θ and the volume V, due to a CCD camera positioned laterally and a backlight. The total evaporation rate is calculated from the volume evolution. The drops have a spherical cap shape because the base radius is always inferior to the capillary length $L_c = \sqrt{(\sigma/\rho g)} = 2.7$ mm where ρ is the fluid density, g is the gravitational constant, and σ is the surface tension.

To ensure the reproducibility of the results, new coatings were used for each experiment, and the surrounding gas phase was renewed at the same time. All of the measurements were performed at least twice to verify the reproducibility of the results. The accuracy of the measurements are 0.5 °C with respect to temperature, 0.1° with respect to the contact angle, 3% with respect to the radius, and 10% with respect to the volume, mass, and global evaporation rate.

IV. RESULTS AND DISCUSSION

A. Influence of the heating temperature of the substrate

1. Hydrophilic situation

In this section, we propose to study the evaporation of a water droplet on an aluminum substrate coated with SiO_x in order to look at the effect of the heating temperature of the substrate T_s on the drop evaporation in a hydrophilic situation ($\theta_0 = 68 \pm 1^\circ$). For all experiments, the triple line is observed to be pinned throughout almost the entire duration of the evaporation process.

The experimental evolutions of the contact angle and the volume are provided in Figs. 3(a) and 3(b), respectively, for substrate temperatures T_s ranging from ambient temperature, 25 °C, up to 75 °C (colored markers). Because the initial contact angle is above 40°, the contact angle decreases nonlinearly with time. Consequently, the volume evolution is also nonlinear due to the influence of the contact angle function [16,32]. These experimental curves appears to be well fit by a quadratic polynomial function [43] (black dash lines). The experimental evaporation time t_F is determined from these extrapolations and is defined as the value of time when the contact angles reach zero degrees. Hence, Fig. 3(c) illustrates the dependence of the evaporation time on the substrate temperature. The variation of the evaporation time t_F is fitted by a power law $t_F = aT_s^{-b}$ as proposed by Girard *et al.* [43] in a numerical investigation. Values of $a = 1.4089 \times 10^6$ and $b = 2.8077$ are obtained with a correlation

TABLE II. Physical properties of liquid and substrate materials used at $T_a = 20$°C.

Parameters	Symbols	Units	Water	Air	Copper	Aluminum	Brass	Bronze	POM
Density	ρ	kg m^{-3}	998	1.2	8920	2700	8450	8770	1420
Specific heat capacity	Cp	J kg^{-1}K^{-1}	4180	1004	380	900	376	377	1500
Thermal conductivity	λ	W m^{-1}K^{-1}	0.61	0.02	401	237	117	50	0.31
Thermal diffusivity	α	($\times 10^{-7}$) m^2 s^{-1}	1.5	217	1183	975	368	151	1.5
Time of heat diffusion	t_{th}	s	7		1	1	3	7	687
Thermal effusivity	β	($\times 10^3$) J K^{-1} m^{-2} s$^{-1/2}$	1.6	6	36.8	24.0	19.94	12.9	0.8
Parallel thermal effusivity	$\beta_\parallel = \frac{\beta_L \beta_S}{\beta_L + \beta_S}$	J K^{-1} m^{-2} s$^{-1/2}$			1525	1491	1470	1414	538

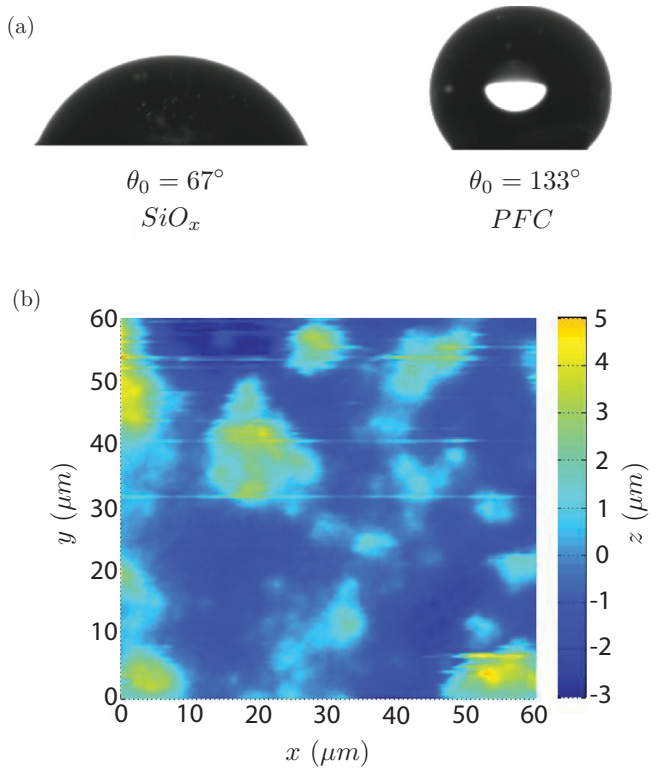

FIG. 2. (Color online) (a) Side view of a 4.2-μL water droplet on the sample surfaces at the initial moment. (b) Atomic force microscopy image of the surface coated with PFC (root mean squared roughness of 1.75 μm).

coefficient close to 1. Consequently, the global evaporation rate $|dm/dt|_g$ increases as the temperature $|dm/dt|_g = \alpha\ {T_s}^{\beta}$ with $\alpha = 1.3315 \times 10^{-13}$, $\beta = 2.9893$ and a correlation coefficient close to 1.

All these experimental data are compared with the quasisteady, diffusion-driven evaporation model, assuming an isothermal droplet at the temperature of the substrate. Indeed, as previously discussed in Sec. II, the comparison of the diffusion time with the evaporation time reveals that the problem is still quasisteady for the entire range of temperatures considered here. Moreover, numerical simulations in similar configurations reveal that, for water droplets evaporating in a substrate at $T_s = 60\,^{\circ}$C at an angle of $\theta = 80°$, even if a small temperature gradient exists at the interface, the temperature of the droplet is close to the temperature of the substrate [43]. The assumption is even more realistic because for the range of contact angles considered, most of the evaporation is performed at the liquid-air interface close to the triple line where the temperature is close to the substrate temperature. The theoretical evolutions of the contact angle and the volume are plotted in the colored dashed lines in Figs. 3(a) and 3(b), with colors corresponding to the substrate temperature.

As previously mentioned in the literature [32,33], this model is a good predictor at ambient temperature: a good agreement on the evolutions of contact angle and volume is observed [see Figs. 3(a) and 3(b)], and a relative deviation of 3.2% is calculated for the evaporation time where $\epsilon_{t_F} = \frac{t_{F_{\text{expt.}}} - t_{F_{th}}}{t_{F_{\text{expt.}}}}$ and the global evaporation rate where $\epsilon_{\dot{m}_g} = \frac{|\dot{m}_g|_{\text{expt.}} - |\dot{m}_g|_{th}}{|\dot{m}_g|_{\text{expt.}}}$.

The model succeeds in describing qualitatively the influence of substrate temperature on the evaporation process. Indeed, as illustrated in Fig. 3, a good prediction of the dynamics of the contact angle, volume, time of evaporation, and global evaporation rate are achieved by the model, which suggests that the model manages to take the global physics of the problem into account. However, one observes a deviation between the model and the experiments, which becomes increasingly important as the temperature increases. Hence, Fig. 3(d) shows that the model always underestimates the evaporation rate and, with an increase in the temperature, the relative deviation increases until reaching 30% at $T_s = 75\,^{\circ}$C. Consequently, the model overestimates the evaporation time and the relative deviation increases with the temperature until reaching 43% at $T_s = 75\,^{\circ}$C. This global underestimation of the global evaporation rate with an increase in the relative deviation is attributed to the effect of buoyant convection in the surrounding air. Indeed, the buoyant convection contribution increases with the temperature and this effect is not included in the model. Recently, numerical investigations revealed the importance of convection in the vapor phase on the evaporation rate. Saada *et al.* [44] showed that the diffusion model underestimates the overall evaporation rate by 8.5% for a wall temperature equal to an ambient temperature of 25 °C and by 27.3% for a wall temperature of 70 °C. The same order of magnitude of the relative deviation is observed between the two studies. This section highlights the contribution of convective transport in the vapor phase during sessile drop evaporation.

2. *Hydrophobic situation*

In this section, the influence of the heating temperature of the substrate during the evaporation of a pinned water droplet is investigated in a hydrophobic situation. The substrate is coated with PFC which results in an initial contact angle of $\theta_0 = 133 \pm 2°$.

The results will be presented in the same way as the previous section. The experimental evolutions of the contact angle and the volume are respectively provided in Figs. 4(a) and 4(c), respectively, for the same range of substrate temperature (from the ambient temperature, 25–75 °C) (colored markers). Because the initial contact angle is more important in this case compared with the previous case, the nonlinearity of the contact angle evolutions increases [32]. Consequently, the nonlinearity of the volume evolutions becomes increasingly important due to the influence of the function of the contact angle [16,32]. Hence, these experimental curves now appear correctly fitted by a polynomial functions of higher degree: degree 6 for the contact angle evolutions and degree 4 for the volume evolutions (black dashed lines). The experimental evaporation time t_F is extracted from these extrapolations and is defined as the time when the contact angles reach 0°. The variation of the evaporation time t_F as a function of the temperature is plotted in Fig. 4(c) and is fitted by a power law $t_F = a{T_s}^{-b}$, with $a = 2.6228 \times 10^6$, $b = 2.2481$, and a correlation coefficient close to 1. The global evaporation rate

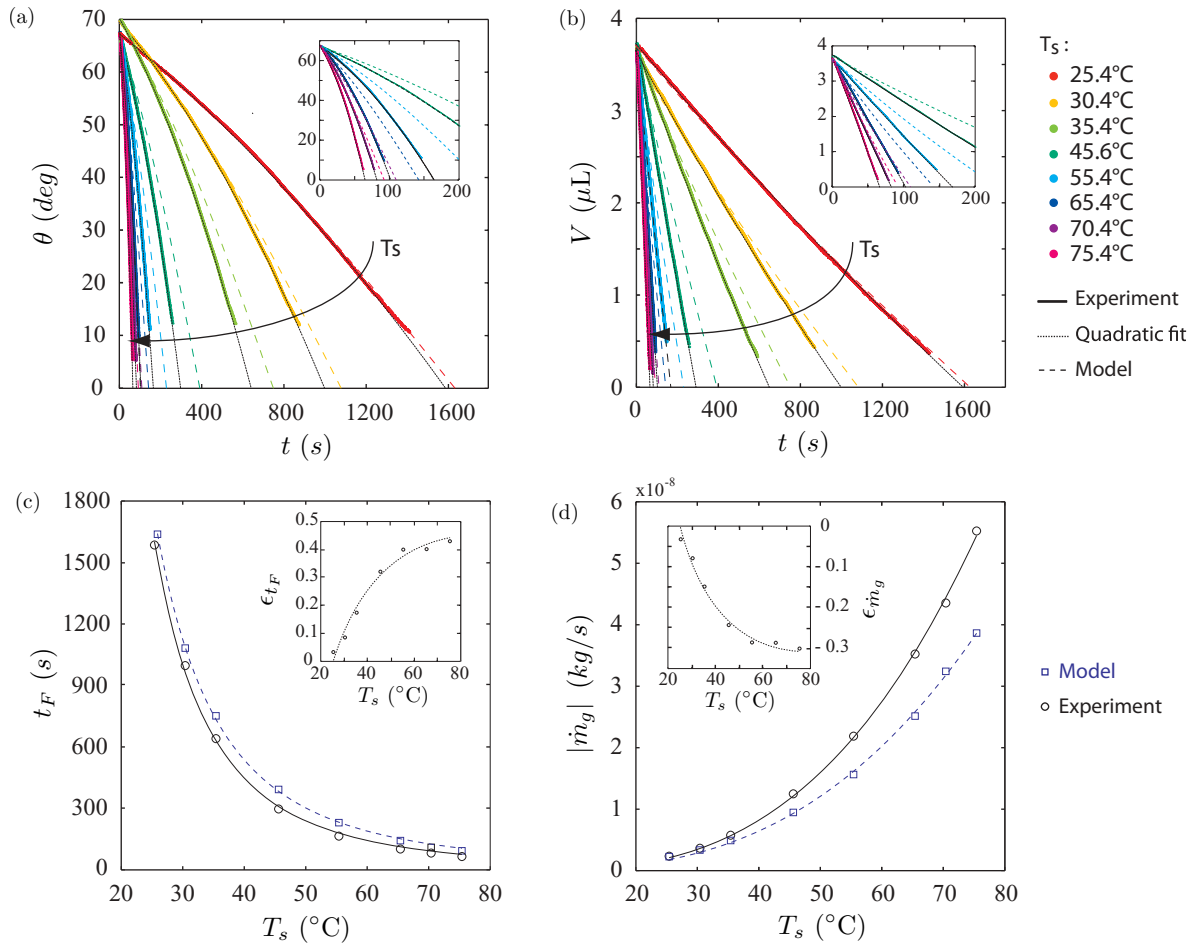

FIG. 3. (Color online) Evaporation of a pinned water droplet on an aluminum substrate coated with SiO_x as a function of the substrate temperature T_s. (a) Contact angle θ variation versus time t. Inset: Zoom. (b) Volume V variation versus time t. Inset: Zoom. (c) Variation of the evaporation time t_F versus the substrate temperature T_s. Inset: Relative deviation of the evaporation time ϵ_{t_F} versus the substrate temperature T_s. (d) Variation of the global evaporation rate $|dm/dt|_g$ versus the substrate temperature T_s. Inset: Relative deviation of the global evaporation rate $\epsilon_{\dot{m}_g}$ versus the substrate temperature T_s. Atmospheric conditions: $T_a = 25.4\,^{\circ}\mathrm{C}$, $P = 101.5$ kPa, $H = 47.5 \pm 1\%$. Drop dimensions: $V = 3.64\ \mu\mathrm{L} \pm 2\%$, $\theta_i = 68 \pm 1^{\circ}$ and $R = 1.44 \pm 0.03$ mm. Complementary information about the equations of fits: in panel (c), (–) $t_F = 1.4089 \times 10^6\ {T_s}^{-2.8077}$, (- -) $t_F = 7.0624 \times 10^6\ {T_s}^{-2.5711}$; in panel (d), (–) $|\dot{m}_g| = 1.3315 \times 10^{-13}\ {T_s}^{2.9893}$, (- -) $|\dot{m}_g| = 1.9157 \times 10^{-13}\ {T_s}^{2.8254}$.

$|dm/dt|_g$ also increases with the same nonlinear evolution with an increase of the temperature $|dm/dt|_g = \alpha\ {T_s}^{\beta}$, with $\alpha = 2.2709 \times 10^{-13}$, $\beta = 2.7438$, and a correlation coefficient close to 1.

The experimental data are compared with the same quasisteady, diffusion-driven evaporation model. The theoretical evolutions of the contact angle and the volume are plotted in colored dashed lines in Figs. 4(a) and 4(b), with colors corresponding to the substrate temperature.

At ambient temperature, a good agreement is observed between the experimental data and the model, as shown in Figs. 4(a) and 4(b) with respect to the evolutions of the contact angle and volume. Moreover, a relative deviation of 3.8% is calculated for the evaporation time and the global evaporation rate.

The model succeeds in qualitatively describing the influence of the substrate temperature on the evaporation process. Indeed, as illustrated in Fig. 4, a good prediction of the dynamics of the contact angle, volume, time of evaporation, and global evaporation rate are exhibited by the model. However, one observes a deviation between the model and the experiments, which becomes increasingly important as the temperature increases. On the whole, in the hydrophobic situation, the model overestimates the evaporation rate and the relative deviation reaches a value of 29.7% at $T_s = 75\,^{\circ}\mathrm{C}$.

Previously, to completely describe the evaporation process, the hydrophilic situation revealed the necessity of accounting for the buoyant convection of transport in the vapor phase because the diffusion-driven evaporation model globally underestimates the global evaporation rate. In the hydrophobic situation, the convective transport is still missing in the model, and yet the model overestimates the global evaporation rate. Hence, the hydrophobic situation highlights another mechanism acting during droplet evaporation that is not included in the model. Indeed, the assumption of droplet isothermia is no longer justifiable in this situation as it was in the hydrophilic one. The thickness of the drop increases and the temperature gradient at the interface is no longer negligible. Considering the local evaporative flux at the liquid-air interface, the maximum of the evaporative flux occurs along the interface

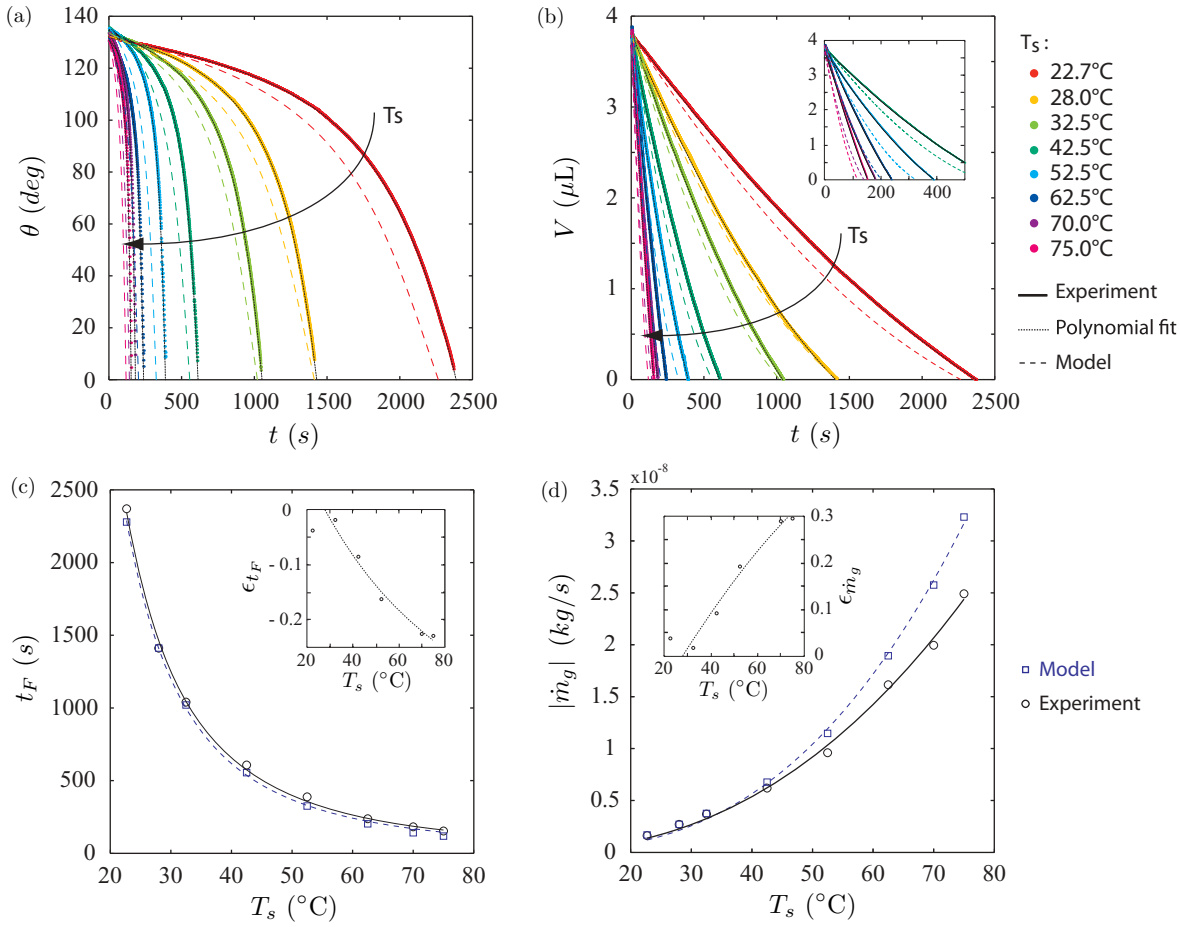

FIG. 4. (Color online) Evaporation of a pinned drop of water on an aluminum substrate coated with PFC as a function of the substrate temperature T_s. (a) Contact angle θ variation versus time t. Inset: Zoom. (b) Volume V variation versus time t. Inset: Zoom. (c) Variation of the evaporation time t_F versus the substrate temperature T_s. Inset: Relative deviation of the evaporation time ϵ_{t_F} versus the substrate temperature T_s. (d) Variation of the global evaporation rate $|dm/dt|_g$ versus the substrate temperature T_s. Inset: Relative deviation of the global evaporation rate $\epsilon_{\dot{m}_g}$ versus the substrate temperature T_s. Atmospheric conditions: $T_a = 23.3 \pm 0.6\,^{\circ}$C, $P = 101.8 \pm 0.1$ kPa, $H = 36.4 \pm 2\%$. Drop dimensions: $V = 3.79\ \mu L \pm 3\%$, $\theta_i = 133 \pm 2^{\circ}$, and $R = 0.72 \pm 0.04$ mm. Complementary information about the equations of fits: the dashed lines are sixth-degree polynomial fits in panel (a) and quadratic polynomial fits in the panel (b); in panel (c), (–) $t_F = 2.6228 \times 10^6\ {T_s}^{-2.2481}$, (- -) $t_F = 3.1285 \times 10^6\ {T_s}^{-2.3124}$ and in panel (d), (–) $|\dot{m}_g| = 2.2709 \times 10^{-13}\ {T_s}^{2.7438}$, (- -) $|\dot{m}_g| = 7.428 \times 10^{-13}\ {T_s}^{2.4086}$.

where the temperature is below the substrate temperature. Hence, the prediction, calculated for an interfacial temperature equal to the substrate temperature, overestimates the real contribution of diffusion transport during evaporation. The deviation due to this assumption appears to be even more important than the contribution of convective transport in the vapor phase. This section clearly reveals the importance of the evaporative cooling effect on the evaporation rate.

3. *Contact angle evolutions*

Figure 5 illustrates the normalized evolutions of the contact angle as a function of the temperature of the substrate for the two situations previously presented, i.e., the hydrophilic case (a) and the hydrophobic case (b). The experimental data (colored lines) are compared with the dimensionless evolution of the contact angle predicted by the quasisteady, diffusion-driven evaporation model (black dashed line). The results show good agreement between the model and the experiments at ambient temperature. However, one observes deviation of the curves with an increase in the temperature of the substrate: the higher the temperature of the substrate, the more deviate the curves. An increase in the deviation is more notable in the hydrophobic case compared with the hydrophilic case. A deviation on the order of 10% is reached between the contact angle at ambient temperature and at 75 °C at $t/t_F = 0.8$ in the hydrophobic situation. Hence, the results reveal the influence of the thermal-linked mechanisms to the contact angle evolution. This influence is not accounted for in the model and could be due to the temperature gradient at the free surface induced by evaporative cooling, which leads to a variation of the saturated vapor concentration along the interface: the temperature gradient is a function of the wettability. This effect may affect the contact angle dynamic as well as the buoyant convection.

B. Influence of the substrate nature

To investigate the influence of the thermal properties of the substrate on droplet evaporation, experiments in which

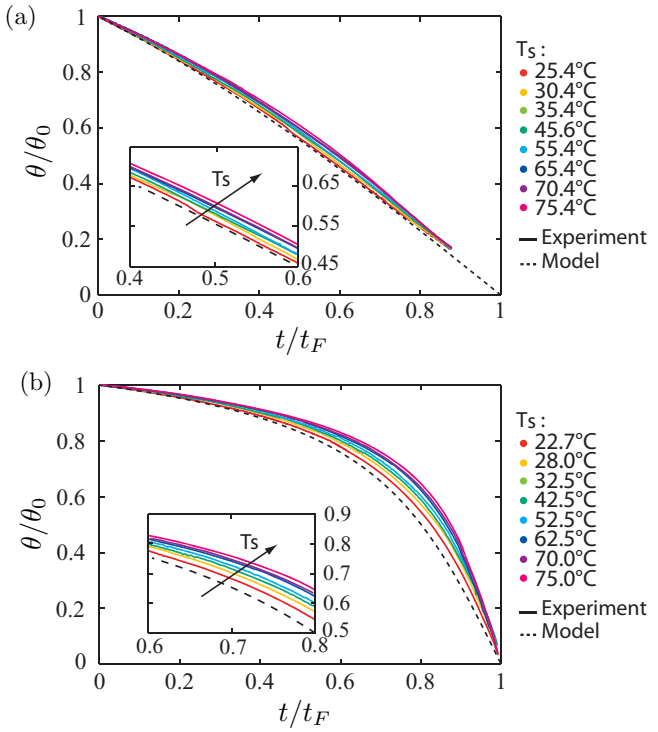

FIG. 5. (Color online) Normalized contact angle θ/θ_0 versus the normalized time t/t_F as a function of the temperature of the substrate for the hydrophilic case (a) and the hydrophobic case (b). Insets: zooms. For complementary information see captions in Fig. 3 for the hydrophilic case and in Fig. 4 for the hydrophobic case.

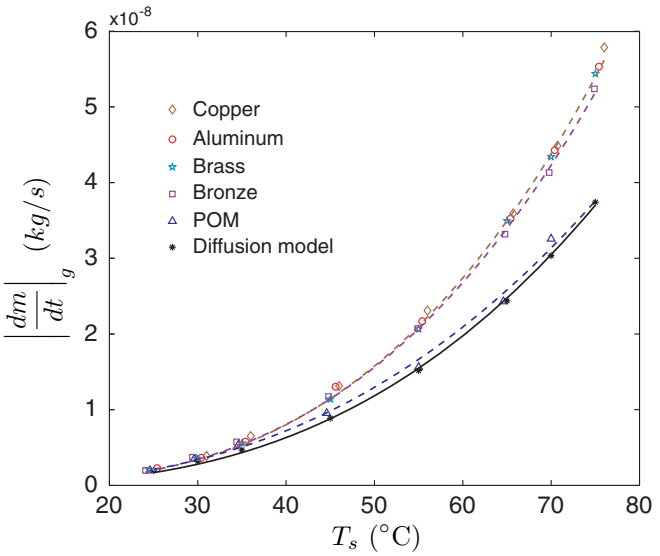

FIG. 6. (Color online) Global evaporation rate $|\frac{dm}{dt}|_g$ of a pinned water droplet versus the temperature of the substrate T_s for various substrate materials. Atmospheric conditions: $T_a = 25 \pm 1\,^\circ$C, $P = 1$ atm $\pm 1\%$, $H = 47.5 \pm 5\%$. Drop dimensions: $V = 3.75 \pm 0.55\mu$L, $\theta_0 = 67.5 \pm 5^\circ$ and $R = 1.44$ mm $\pm 10\%$. Complementary information about the equations of fits: (brown - -) power law fit of copper points $|\dot{m}_g| = 1.0974 \times 10^{-13}\ {T_s}^{3.0355}$, (purple - -) power law fit of bronze points $|\dot{m}_g| = 1.4312 \times 10^{-13}\ {T_s}^{2.965}$, (blue - -) power law fit of POM points $|\dot{m}_g| = 4.4651 \times 10^{-13}\ {T_s}^{2.6267}$, (black –) power law fit of the diffusion model $|\dot{m}_g| = 1.9493 \times 10^{-13}\ {T_s}^{2.8151}$.

the nature of the substrate was changed were conducted. All substrates were coated with SiO_x to perform these experiments with the same physical chemistry of the surface. All evaporation considered here occurs in the hydrophilic situation $\theta_0 = 67.5 \pm 5^\circ$ with the pinning of the triple line. Figure 6 presents the global evaporation rate as a function of the substrate temperature for various substrates including copper, aluminum, brass, bronze, and POM. The experimental data are compared with the quasisteady, diffusion-driven evaporation model calculated for the median value of each parameter.

The global evaporation rate is found to be, respectively, higher for substrates with higher thermal conductivity. It is worth noting however that all curves for metallic substrates (copper, aluminum, brass, bronze) are grouped as if there is virtually no difference despite an order of magnitude difference in thermal conductivity. This observation was already performed by David *et al.* [38] about evaporating droplets at ambient temperatures.

When the substrate is at ambient temperature, the experiences reveal a median global evaporation rate of $|\frac{dm}{dt}|_g = 2.18 \pm 0.14 \times 10^{-9}$ kg s^{-1} for metallic substrates. The deviation is below the uncertainty measurement of the global evaporation rate. A difference of 14% on the median value of the global evaporation rate is noticed between metallic and polymeric substrates. A difference of the same order of magnitude was reported in the investigation of David *et al.* [38]. The authors explained the decrease in the evaporation rate by an important cooling effect when the substrate is thermally insulating.

The difference in the global evaporation rate increases with the increase in the substrate temperature and reaches 53.9% at $T_s = 75\,^\circ$C between a droplet evaporating onto a copper or a POM substrate. The increase in the evaporation rate due to the increase of the substrate temperature amplifies the effects of the thermal properties influence.

These results highlight the crucial role of the thermal properties of the substrate. Indeed, due to evaporation process (latent heat), energy is consumed by the droplet and a part of this energy is supplied from the surrounding environment. Considering the thermal conductivities of the air and the substrate materials (see Table II), the energy should be mainly brought by heat conduction from the substrate to the droplet. Instead of considering these results through the thermal conductivity of the substrate (as it is usually done in the literature), it is preferable to use the concept of thermal effusivity $\beta = \sqrt{\lambda \rho C_p}$. The thermal effusivity characterizes the ability of a material to change temperature when it absorbs or supplies heat energy. It accounts for variation of the surface temperature due to variation in heat flux density at its surface. The thermal effusivity is a broader concept because it includes the change of temperature by heat storage and heat conduction; hence, it also allows us to take unsteady process into account. Considering the characteristic time scales of thermal conduction in the system (see Table II), the heat transfer cannot always be considered as quasistationary state. Indeed, the POM substrate is characterized by a diffusion time of 687 s which is not negligible compared with the lifetime of the droplets in the experiments. The thermal effusivity

of the several materials is provided in Table II. The same interpretation is performed with the thermal effusivity as the thermal conductivity. Hence, the data reveal that the more effusive a substrate, the more important the evaporation rate. However, there is virtually no difference of behavior for the metallic substrates whereas an important difference is noted compared with the polymer. Indeed, the highly effusive substrates are weakly sensitive to the evaporation on its surface which leads to a surface temperature close to the imposed temperature whereas the lowly effusive substrates are very sensitive to the evaporation on its surface which leads to a lower surface temperature. Consequently, the global evaporation rate is lower in the situation of lowly effusive substrate.

However, the only consideration of the substrate thermal effusivity does not satisfactorily explain the similar values of global evaporation rates for the metallic substrates. The repartition of curves as a function of the substrate thermal properties is correctly explained by the equivalent thermal effusivity, which corresponds to the parallel thermal effusivity of the two materials in contact, i.e., the drop and the substrate. Indeed, previous studies were performed considering the contact between a liquid drop at temperature T_a and a wall at temperature T_s [50]. In the first stage, the temperature of the contact is determined by the theory of heat transfer between two semi-infinite materials, $T_c = \frac{\beta_L T_L + \beta_S T_s}{\beta_L \beta_S}$, and the heat flux received by the drop is $q_L = \frac{\beta_L}{\sqrt{\pi t}}(T_c - T_a) = \frac{\beta_{//}}{\sqrt{\pi t}}(T_s - T_a)$, with the equivalent thermal effusivity $\beta_{//} = \frac{\beta_L \beta_S}{\beta_S + \beta_L}$ where the subscripts S and L indicates the materials considered, respectively, solid and liquid. Considering the parallel thermal effusivity for the materials considered in these study (see Table II), the parallel thermal effusivity for the metallic substrate-water couples are of the same order of magnitude and a ratio of 2.8 is obtained between the copper-water and POM-water couples. Hence, the parallel thermal effusivity describes the equivalent behavior obtained for metallic substrates and the important difference with the polymeric substrate. The ratio of the equivalent thermal effusivities between the copper-water and POM-water couples is of the same order of magnitude but slightly overpredicted the ratio of the global evaporation rate between the same materials. The difference is acceptable considering the uncertainties of measurements and the difference in time scales considered between the theory and the experiments.

All of the experimental results are compared with the quasisteady, isothermal, diffusion model of evaporation. The model describes qualitatively the influence of the substrate temperature on the global evaporation rate. However, the model does not include any of the thermal properties of the liquid and the substrate. As describe previously in the specific case of the aluminum substrate, the model underestimates the global evaporation rate for the highly effusive substrates. The relative deviation increases with the increase of the temperature until reaching 58.9% at $T_s = 75\,^{\circ}\mathrm{C}$ for the copper substrate. The curve obtained for the lowly effusive substrate is close to the model by chance. It suggests that the contribution of the increase of the evaporation rate by the buoyant convection in the vapor transport is counterbalanced by the decrease in the energy transport on the substrate and the evaporative cooling effect.

V. CONCLUSION

The influence of the thermal effects of the substrate on the behavior of a pinned sessile water droplet evaporating into air has been investigated in the hydrophilic and hydrophobic cases. Hence, the effect of the substrate temperature on geometrical evolutions, time of evaporation, and the global evaporation rate have been studied, as well as the influence of the thermal properties of the substrate on the global evaporation rate. Experimental results are compared with the quasisteady, diffusion-driven evaporation model, which is implemented with the influence of the temperature and assumes isothermia of the interface at the substrate temperature. The results highlight a favorable agreement between the model and the experimental data at ambient temperatures for most situations considered here. However, with an increase in temperature, the contribution of mechanisms linked with thermal effects becomes increasingly important. Indeed, the global evaporation rate appears clearly influenced by the thermal effusivity of the substrate, and the contact angle evolution is modified with an increase in temperature. The theoretical model succeeds in qualitatively describing the influence of the substrate temperature on the evaporation process. However, comparison with the experimental data highlights the need for a more accurate model that accounts for the buoyant convection in the vapor transport and the evaporative cooling and thermal conduction between the droplet and the substrate.

ACKNOWLEDGMENTS

We would like to thank J. Gavillet from CEA LITEN, Grenoble, France, for performing nanocoatings, F. Rigollet for fruitful discussions, and M. Hadj for carrying out preliminary experiments. Fundings from Agence Nationale de la Recherche (Project NanoSurf ANR- 37509-BLAN-0093-03), Centre National d'Etudes Spatiales (Project "Sessile Drop Evaporation"), and Carnot STAR (Project "Nano Phase Change") are gratefully acknowledged.

[1] J. Jing, J. Reed, J. Huang, X. Hu, V. Clarke, J. Edington, D. Housman, T. S. Anantharaman, E. J. Huff, B. Mishra, B. Porter, A. Shenker, E. Wolfson, C. Hiort, R. Kantor, C. Aston, and D. C. Schwartz, Proc. Natl. Acad. Sci. **95**, 8046 (1998).

[2] R. Blossey, Nat. Mater. **2**, 301 (2003).

[3] A. F. M. Leenaars, J. A. M. Huethorst, and J. J. Van Oekel, Langmuir **6**, 1701 (1990).

[4] T. P. Bigioni, X. Lin, T. T. Nguyen, E. I. Corwin, T. A. Witten, and H. M. Jaeger, Nat. Mater. **5**, 265 (2006).

[5] D. Kim, S. Jeong, B. K. Park, and J. Moon, Appl. Phys. Lett. **89**, 264101 (2006).

[6] J. Park and J. Moon, Langmuir **22**, 3506 (2006).

[7] J. Boneberg, F. Burmeister, C. Schafle, and P. Leiderer, Langmuir **13**, 7080 (1997).

[8] T. Ondarcuhu and C. Joachim, Europhys. Lett. **42**, 215 (1998).
[9] T. Kawase, H. Sirringhaus, R. H. Friend, and T. Shimoda, Adv. Mater. **13**, 1601 (2001).
[10] D. J. Norris, E. G. Arlinghaus, L. Meng, R. Heiny, and L. E. Scriven, Adv. Mater. **16**, 1393 (2004).
[11] T. Yakhno, J. Colloid Interface Sci. **318**, 225 (2008).
[12] D. Brutin, B. Sobac, B. Loquet, and B. Sampol, J. Fluid Mech. **667**, 85 (2011).
[13] B. Sobac and D. Brutin, Phys. Rev. E **84**, 011603 (2011).
[14] R. G. Picknett and R. Bexon, J. Colloid Interface Sci. **61**, 336 (1977).
[15] R. D. Deegan, O. Bakajin, T. F. Dupont, G. Huber, S. R. Nagel and T. A. Witten, Phys. Rev. E **62**, 756 (2000).
[16] H. Hu and R. G. Larson, J. Phys. Chem. B **6**, 1334 (2002).
[17] Y. O. Popov, Phys. Rev. E **71**, 036313 (2005).
[18] D. Quéré, Annu. Rev. Mater. Res. **38**, 71 (2008).
[19] D. Bonn, J. Eggers, J. Indekeu, J. Meunier, and E. Rolley, Rev. Mod. Phys. **81**, 739 (2009).
[20] J. Yu, X. Zhao, Q. Zhao, and G. Wang, Mater. Chem. Phys. **68**, 253 (2001).
[21] T. Onda, S. Shibuichi, N. Satoh, and K. Tsujii, Langmuir **12**, 2125 (1996).
[22] L. Feng, S. Li, Y. Li, H. Li, L. Zhang, J. Zhai, Y. Song, B. Liu, L. Jiang, and D. Zhu, Adv. Mater. **14**, 1857 (2002).
[23] M. Reyssat, J. M. Yeomans and D. Quéré, Europhys. Lett. **81**, 26006 (2008).
[24] A. Tuteja, W. Choi, M. Ma, J. M. Mabry, S. A. Mazzella, G. C. Rutledge, G. H. McKinley, and R. E. Cohen, Science **318**, 1618 (2007).
[25] A. Mamur, Langmuir **24**, 7573 (2008).
[26] L. Joly and T. Biben, Soft Matter **5**, 2549 (2009).
[27] H. Y. Erbil, G. McHale, and M. I. Newton, Langmuir **18**, 2636 (2002).
[28] K. S. Birdi, D. T. Vu, and A. Winter, J. Phys. Chem. **93**, 3702 (1989).
[29] S. M. Rowan, M. I. Newton and G. McHale, J. Phys. Chem. **99**, 13268 (1995).
[30] C. Bourges-Monnier and M. Shanahan, Langmuir **11**, 2820 (1995).
[31] M. Cachile, O. Benichou, C. Poulard, and A. M. Cazabat, Langmuir **18**, 8070 (2002).
[32] B. Sobac and D. Brutin, Langmuir **27**, 14999 (2011).
[33] H. Gelderblom, A. G. Marin, N. Nair, A. van Houselt, L. Lefferts, J. H. Snoeijer, and D. Lohse, Phys. Rev. E **83**, 026306 (2011).
[34] S. A. Kulinich and M. Farzaneh, Appl. Surf. Sci. **255**, 4056 (2009).
[35] L. Grandas, C. Reynard, R. Santini, and L. Tadrist, Int. J. Therm. Sci. **44**, 137 (2005).
[36] D. H. Shin, S. H. Lee, J. Y. Jung, and J. Y. Yoo, Microelec. Eng. **86**, 1350 (2009).
[37] W. D. Ristenpart, P. G. Kim, C. Domingues, J. Wan, and H. A. Stone, Phys. Rev. Lett. **99**, 234502 (2007).
[38] S. David, K. Sefiane, and L. Tadrist, Colloids Surf. A **198**, 108 (2007).
[39] G. J. Dunn, S. K. Wilson, B. R. Duffy, S. David, and K. Sefiane, J. Fluid Mech. **623**, 329 (2009).
[40] K. Sefiane and R. Bennacer, J. Fluid Mech. **667**, 260 (2011).
[41] G. J. Dunn, S. K. Wilson, B. R. Duffy, and K. Sefiane, Phys. Fluids **21**, 052101 (2009).
[42] E. Crafton and W. Black, Int. J. Heat Mass Transfer **47**, 1187 (2004).
[43] F. Girard, M. Antoni, S. Faure, and A. Steinchen, Colloids Surf. A **323**, 36 (2008).
[44] M. A. Saada, S. Chikh, and L. Tadrist, Phys. Fluids **22**, 112115 (2010).
[45] C. Sodtke, V. S. Ajaev, and P. Stephan, Heat Mass Transfer **43**, 649 (2007).
[46] N. Shahidzaneh-Bonn, S. Rafa, A. Azouni, and D. Bonn, J. Fluid Mech. **549**, 307 (2006).
[47] N. N. Lebedev, *Special Functions and their Applications* (Prentice-Hall, Englewood Cliffs, NJ, 1965).
[48] F. Girard, M. Antoni, S. Faure, and A. Steinchen, Langmuir **22**, 11085 (2006).
[49] H. T. Phan, N. Caney, P. Marty, S. Colasson, and J. Gavillet, Int. J. Heat Mass Transfer **52**, 5459 (2009).
[50] T. Loulou and J. P. Bardon, Rev. Gen. Therm. **36**, 682 (1997).